High Power Laser Science and Engineering, (2020), Vol. 8, e6, 5 pages.
doi:10.1017/hpl.2019.54

HIGH POWER LASER SCIENCE AND ENGINEERING

RESEARCH ARTICLE

Rapid growth of a long-seed KDP crystal

Duanyang Chen[1,2], Bin Wang[1], Hu Wang[1], Xiangyu Zhu[3], Ziyuan Xu[1], Yuanan Zhao[1], Shenghao Wang[1], Kaizao Ni[1], Lili Zheng[3], Hui Zhang[4], Hongji Qi[1], and Jianda Shao[1]

[1]*Key Laboratory of Materials for High Power Laser, Shanghai Institute of Optics and Fine Mechanics, Chinese Academy of Sciences, Shanghai 201800, China*

[2]*Center of Materials Science and Optoelectronics Engineering, University of Chinese Academy of Sciences, Beijing 100049, China*

[3]*School of Aerospace Engineering, Tsinghua University, Beijing 100084, China*

[4]*Department of Engineering Physics, Tsinghua University, Beijing 100084, China*

(Received 24 September 2019; revised 13 November 2019; accepted 11 December 2019)

Abstract

To reduce the seed length while maintaining the advantages of the cuboid KDP-type crystal, a long-seed KDP crystal with size 471 mm × 480 mm × 400 mm is rapidly grown. With almost the same high cutting efficiency to obtain third harmonic generation oriented samples, this long-seed KDP-type crystal can be grown with a shorter seed than that of the cuboid KDP-type crystal. The full width at half maximum of the high-resolution X-ray diffraction of the (200) crystalline face is 28.8 arc seconds, indicating that the long-seed KDP crystal has good crystalline quality. In the wavelength range of 377–1022 nm, the transmittance of the long-seed KDP crystal is higher than 90%. The fluence for the 50% probability of laser-induced damage (LID) is 18.5 J/cm^2 (3 ns, 355 nm). Several test points survive when the laser fluence exceeds 30 J/cm^2 (3 ns, 355 nm), indicating the good LID performance of the long-seed KDP crystal. At present, the growth of a long-seed DKDP crystal is under way.

Keywords: KDP crystal; long-seed; rapid growth

1. Introduction

The high-power lasers used in the inertial confinement fusion (ICF) system worldwide need large KDP-type crystals as nonlinear crystals on account of their exceptional properties[1–6]. The major limitation to growing such large KDP-type crystals by the traditional method is the slow growth rate, leading to a growth cycle of 1–2 years[7–11]. Fortunately, the 'point-seed' rapid growth method was developed in the 1980s[12, 13]. For the KDP-type crystals produced by the 'point-seed' rapid growth method, all prismatic faces and pyramidal faces develop under high supersaturated solutions[14–17]. In addition, a pyramid–prism (PY–PR) boundary is generated when different kinds of crystallographic faces are sewn together[18–21]. By the orthogonal polarization interferometry technology, $\Delta(n_e–n_o)$ maps containing the PY–PR boundary were easily obtained, and the distortion near the PY–PR boundary was reported to be detrimental to efficient frequency tripling and phase matching[22, 23]. More recently, a cuboid DKDP crystal was rapidly grown[24]. Without a pyramidal sector, the cuboid DKDP crystal had high cutting efficiency to obtain third harmonic generation (THG)-oriented samples for ICF. However, in practice, it is not always easy to get a long seed to grow a large cuboid KDP-type crystal. Therefore, it is of practical significance to reduce the length of the seed while maintaining the advantages of the cuboid KDP-type crystal.

In this study, a long-seed KDP crystal was rapidly grown. With almost the same high cutting efficiency to obtain THG-oriented samples, this long-seed KDP-type crystal can grow from a seed that is shorter than that of the cuboid KDP-type crystal. Then the crystalline quality, transmittance performance, laser-induced damage (LID) property and LID morphology of the long-seed KDP crystal were investigated.

2. Experimental setup

2.1. Crystal growth

The long-seed KDP crystal was rapidly grown in a self-developed 2000 L growth apparatus configured as an effi-

Correspondence to: H. Qi and J. Shao, No. 390 Qinghe Road, Jiading District, Shanghai 201800, China. Email: qhj@siom.ac.cn (H. Qi); jdshao@mail.shcnc.ac.cn (J. Shao)

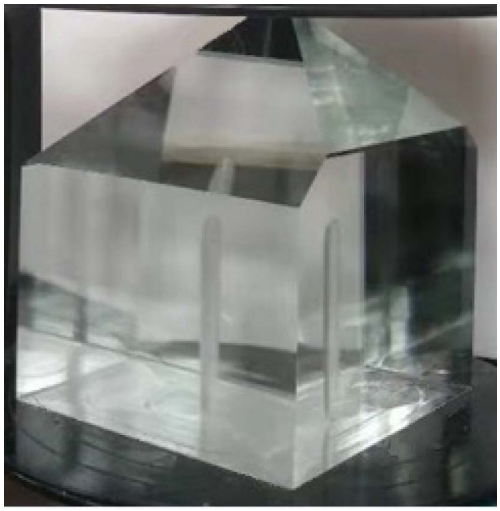

Figure 1. Long-seed KDP crystal with size 471 mm × 480 mm × 400 mm.

cient continuous filtration system (CFS)[25, 26]. A long KDP seed with size 20 mm×20 mm×260 mm was fixed on a crystal carrier, and the length direction of the seed crystal was the [001] crystallography direction. During crystal growth, the supersaturation of the solution was approximately 5%, and the crystal carrier was rotated in alternative cycles[27, 28]. After 70 days, a long-seed KDP crystal with dimensions 471 mm×480 mm×400 mm and weight 254 kg was grown, as shown in Figure 1. It is worth mentioning that there is no visible defect in the long-seed KDP crystal. In addition, the growth of a long-seed DKDP crystal is currently under way.

2.2. Characterization techniques

To evaluate the properties of the long-seed KDP crystal, the high-resolution X-ray diffraction (HRXRD) of an X-cut sample from this crystal was carried out[29]. The transmission spectrum of a THG-oriented sample cut from the long-seed KDP crystal was tested using a Lambda 1050 spectrometer[18]. The LID threshold (LIDT) at 355 nm of the THG-oriented sample was investigated under a Nd:YAG laser[30]. The LID scattering image of the THG-oriented sample was captured by an online microscope system mounted on the laser damage facility, and the morphology of the LID bulk was observed by an offline polarization microscope[31].

3. Results and discussion

3.1. Advantages of cut THG-oriented samples

The THG-oriented samples cut from the cuboid KDP-type crystal and the long-seed KDP-type crystal are shown in Figure 2. As in our previous work, the number N of THG-oriented samples cut from the cuboid KDP-type crystal follows the formulas below[24]:

$$(T\sin\alpha + V)\times 2 + s = L, \tag{1}$$

$$W\sin\alpha + T\cos\alpha + IN/2 = H, \tag{2}$$

where L, W and T are the length, width and thickness of the largest THG-oriented sample that can be cut from the cuboid KDP-type crystal. The height of the cuboid KDP-type crystal is H, the width of the seed is s and the phase-matching angle of the THG-oriented sample is α. The parameters V and I represent the width of the projection of the sample on the horizontal plane and the spacing of the adjacent two samples in the direction of height, respectively.

For simplicity, α and s are approximately equal to 60° and 15 mm, respectively; V and I are equal to $W\cos\alpha$ and $T/\cos\alpha$, respectively. The above two formulas can be simplified as follows:

$$(0.886T + 0.5W)\times 2 + 15 = L, \tag{3}$$

$$0.886W + 0.5T + NT = H. \tag{4}$$

Therefore, to get 10 ($N = 10$) THG-oriented samples with size 460 mm × 430 mm × 10 mm ($W = 430$, $T = 10$, $L = (0.886T + 0.5W)\times 2 + 15 \approx 460$), the cuboid KDP-type crystal should grow to size of 460 mm × 460 mm × 486 mm ($H = 0.886W + 0.5T + NT = 486$), and the length of the seed should also be 486 mm.

For the long-seed KDP-type crystal, the growth rate in the horizontal and vertical directions is approximately 3:2, according to the crystal grown in this study. Equations (1)–(4) are also applicable to the long-seed KDP-type crystal, with only minor corrections in height. Equation (2) can be approximately changed to

$$W\sin\alpha + T\cos\alpha + IN/2 + T = H. \tag{5}$$

Therefore, to get 10 ($N = 10$) THG-oriented samples with size 460 mm × 430 mm × 10 mm, the long-seed KDP-type crystal should grow to size 460 mm × 460 mm × 496 mm ($H = 0.886W + 0.5T + NT + T = 496$). Since the prismatic face grew by about 222 mm, the crystal grew by approximately 148 mm in the length direction. So a seed with length 348 mm is sufficient. As mentioned above, the length of the seed is 486 mm for the cuboid KDP-type crystal. For the long-seed KDP-type crystal, the seed crystal can be shortened by 138 mm in this case.

3.2. Crystalline quality of the long-seed KDP crystal

The HRXRD pattern of the (200) crystalline face cut from the long-seed KDP crystal is shown in Figure 3. The full width at half maximum (FWHM) of the HRXRD is 28.8 arc seconds, indicating that the long-seed KDP crystal has good

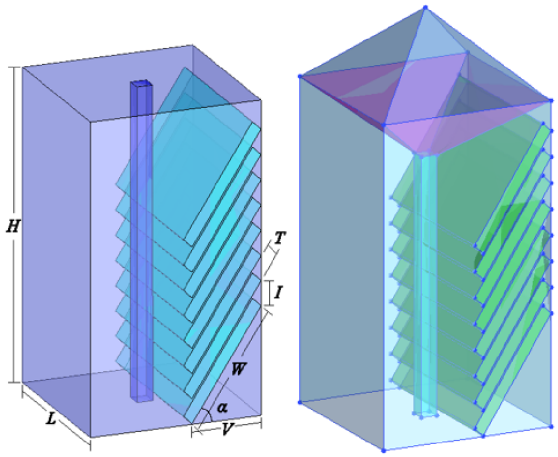

Figure 2. THG-oriented samples cut from the cuboid KDP-type crystal (left) and the long-seed KDP-type crystal (right).

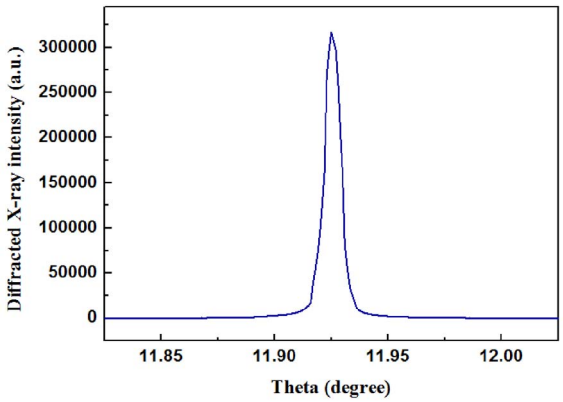

Figure 3. HRXRD pattern of the long-seed KDP crystal.

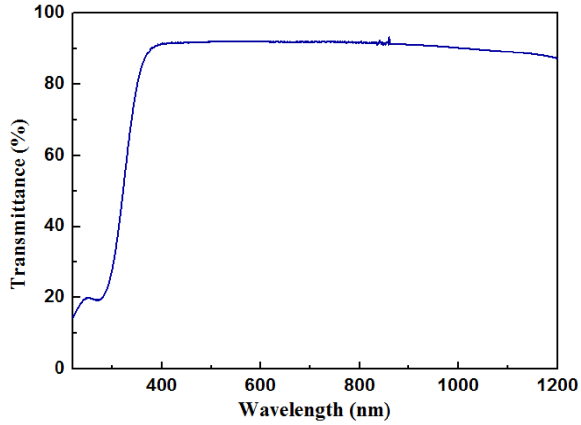

Figure 4. Transmittance of the long-seed KDP crystal.

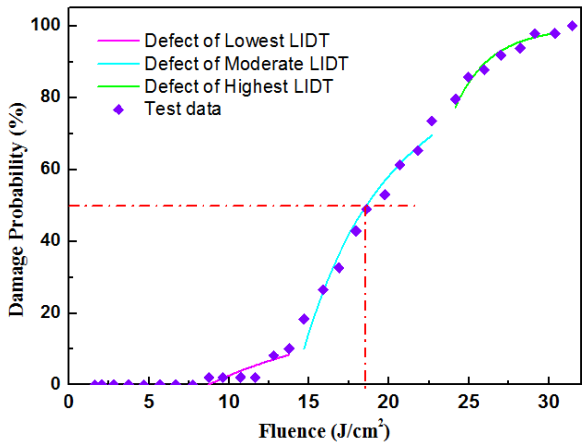

Figure 5. LIDT of the long-seed KDP crystal.

crystalline quality. More details about the testing can be found in other articles[18, 24]. As defined by the plane wave dynamic theory of X-ray diffraction, a smaller value of FWHM indicates better crystallinity[32, 33]. For the cuboid DKDP crystal, the FWHM of the HRXRD is also 28.8 arc seconds, indicating that there is no essential difference in crystalline quality between the cuboid KDP-type crystal and the long-seed KDP-type crystal[24].

3.3. Transmittance of the long-seed KDP crystal

The transmission spectrum of a THG-oriented sample of the long-seed KDP crystal is shown in Figure 4. The vibration near 860 nm was caused by switching the detectors of the spectrometer at this wavelength. In the wavelength range of 377–1022 nm, the transmittance is higher than 90%, which is almost the same as that of the cuboid DKDP crystal. The transmittance at 355 nm is 82.9%, a little higher than that of the cuboid DKDP crystal[24]. The various factors responsible for the origin and influence of optical transmittance can be found from peer-reviewed literature[34–36].

3.4. Laser-induced damage property

The LID property at 355 nm of the THG-oriented sample cut from the long-seed KDP crystal is shown in Figure 5. The effective area of the laser spot is 0.26 mm^2. The fluence for the 50% probability of LID is 18.5 J/cm^2 (3 ns, 355 nm), 38% higher than that of the cuboid DKDP crystal[24]. Several test points survive when the laser fluence exceeds 30 J/cm^2 (3 ns, 355 nm), indicating the good LID property of the long-seed KDP crystal.

A model is used to quantify the LID property of the long-seed KDP crystal[37, 38]. In Figure 5, three types of defects are fitted. The fitted LIDT and density of different kinds of defects are shown in Table 1. The density is 0.063 mm^{-3} for the defect that has the lowest LIDT, indicating that defects that can easily induce damage under 355 nm in the long-seed KDP crystal are rare. Some extrinsic factors such as

Table 1. Fitting of different kinds of defects.

Defect type	Fitted LIDT (J/cm^2 at 3 ns, 355 nm)	Fitted density (mm^{-3})
Lowest LIDT	8.72	0.063
Moderate LIDT	14.64	0.748
Highest LIDT	23.72	2.644

Figure 6. LID scattering image at 30 J/cm^2 (3 ns, 355 nm).

incident photon energy, pulse width and polarization mode and intrinsic factors such as thermal expansion coefficient, electron avalanche breakdown and nonlinear absorption effects play decisive roles in laser damage properties of crystalline materials. Detailed explanations are given in Refs. [39–41].

3.5. Laser-induced damage morphology

Illuminated by a 532 nm probe laser, the LID scattering image of the THG-oriented sample is recorded by an online microscope system mounted on the laser damage facility. The microscope is placed orthogonally to the propagation direction of the 355 nm laser. Once the damage happens, the microscope immediately captures the LID scattering image. An LID scattering image at 30 J/cm^2 (3 ns, 355 nm), is shown in Figure 6, with length about 10 mm, which is also the thickness of the sample. Even at such a high fluence, only three damage points appear within 10 mm, indicating that the long-seed KDP crystal has good damage resistance. Although it looks like six scattering points in the figure, there are actually only three LID points. Because of birefringence, the scattered light of each LID point is split into two beams (namely the o light and e light), forming two scattering points in the microscope.

The morphology of the damage points in Figure 6 is observed by an offline polarization microscope. The morphology of damage points in Figure 7 from left to right shows exactly the same points as in Figure 6. In Figure 7, all the damage points consist of a core, a distortion zone around the core and cracks extending from the core[42, 43]. Because the sample did not rotate when testing the morphology of the three points, all the cracks extend in only two directions, which should be the directions of the crystalline axes[44–46]. An approach to evaluate damage performance provides statistics on damage pinpoint density, size and morphology as a function of fluence, wavelength and pulse duration and relates that to the resulting beam obscuration[47]. The power limitation was found to play a vital role in the use of rapidly grown KDP-type crystals in the ICF system.

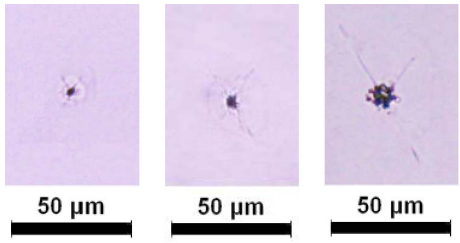

Figure 7. Morphology of the LID bulks in Figure 6.

4. Conclusions

Despite being the subject of study for more than 30 years, rapidly grown KDP-type crystals are still grown from a 'point seed'. In this study, a long-seed KDP crystal with size 471 mm × 480 mm × 400 mm was rapidly grown. With almost the same high cutting efficiency to obtain THG-oriented samples, this long-seed KDP-type crystal can grow from a seed that is shorter than that of the cuboid KDP-type crystal proposed in the recently published literature[24]. For example, to get 10 THG-oriented samples with size 460 mm × 430 mm × 10 mm, the size of the seed should be at least 486 mm for the cuboid KDP-type crystal, while it is just 348 mm for the long-seed KDP-type crystal. Therefore, it is of practical significance since it is not always easy to get a long seed to grow a large cuboid KDP-type crystal. The long-seed KDP crystal also exhibits good crystalline quality since the FWHM of HRXRD is the same as that of the cuboid DKDP crystal[24]. As to the transmission and the LID performance, the long-seed KDP crystal is even better than the cuboid DKDP crystal[24]. Furthermore, new seeds with much longer size in the [001] crystallography direction than the original seed can be taken from the pyramidal portion down through the prismatic portion. In addition, because the carrier has a height greater than that of the long seed, there is no need to replace the carrier for a different seed with that of different height. For the cuboid KDP-type crystal, once the height of the carrier is set, the length of the seed must be equal to the height of the carrier. Therefore, the long-seed KDP-type crystal is more promising than the cuboid KDP-type crystal in engineering application.

Acknowledgement

This work was supported by the National Natural Science Foundation of China (No. 11535010).

References

1. J. J. De Yoreo, A. K. Burnham, and P. K. Whitman, Int. Mater. Rev. **47**, 113 (2002).
2. P. Huang, J. Ding, D. Wang, H. Liu, L. Xu, X. Li, B. Wang, G. Liu, and S. Wang, CrystEngComm **21**, 1329 (2019).
3. J. Piquard, J. Zaccaro, B. Pintault, C. Maunier, and A. Ibanez, CrystEngComm **21**, 372 (2019).
4. P. Huang, S. Wang, D. Wang, H. Liu, G. Liu, and L. Xu, CrystEngComm **20**, 3171 (2018).
5. C. Sun and D. Xue, CrystEngComm **15**, 10445 (2013).
6. X. Cai, X. Lin, G. Li, J. Lu, Z. Hu, and G. Zheng, High Power Laser Sci **7**, e46 (2019).
7. D. Wang, T. Li, S. Wang, J. Wang, Z. Wang, J. Ding, W. Li, C. Shen, G. Liu, and P. Huang, CrystEngComm **18**, 9292 (2016).
8. I. Khan, S. Kalainathan, M. I. Baig, M. Shkir, S. Alfaify, H. A. Ghramh, and M. Anis, Materials Science-Poland **36**, 662 (2018).
9. M. Anis, G. G. Muley, M. I. Baig, G. Rabbani, H. A. Ghramhans, and S. P. Ramteke, Optik **178**, 752 (2019).
10. M. I. Baig, M. Anis, and G. G. Muley, Opt. Mater. **72**, 1 (2017).
11. W. Li, G. Yu, S. Wang, J. Ding, X. Xu, Q. Gu, D. Wang, and P. Huang, RSC Adv. **7**, 17531 (2017).
12. N. Zaitseva and L. Carman, Prog. Cryst. Growth Charact. Mater. **43**, 1 (2001).
13. D. Wang, C. Shen, J. Lan, P. Huang, Z. Cui, T. Kang, Y. Niu, S. Wang, J. Wang, and R. I. Boughton, J. Alloys Compd. **790**, 212 (2019).
14. T. A. Land, T. L. Martin, S. Potapenko, G. T. Palmore, and J. J. De Yoreo, Nature **399**, 442 (1999).
15. H. Tu, Y. Zhao, Y. Yue, F. Fan, and Z. Hu, CrystEngComm **17**, 6669 (2015).
16. R. Hawley-Fedder, P. Geraghty, S. Locke, M. McBurney, M. Runkel, T. Suratwala, S. Thompson, P. Wegner, and P. Whitman, Proc. SPIE **5341**, 121 (2004).
17. M. Pommies, D. Damiani, B. Bertussi, J. Capoulade, H. Piombini, J. Y. Natoli, and H. Mathis, Opt. Commun. **267**, 154 (2006).
18. D. Chen, B. Wang, H. Wang, Y. Bai, N. Xu, B. Li, H. Qi, and J. Shao, CrystEngComm **21**, 1482 (2019).
19. R. A. Negres, N. P. Zaitseva, P. DeMange, and S. G. Demos, Proc. SPIE **6403**, 64031S (2006).
20. A. Surmin, F. Guillet, S. Lambert, D. Damiani, and M. Pommiès, Proc. SPIE **5991**, 59911W (2005).
21. M. Yan, R. A. Torres, M. J. Runkel, B. W. Woods, I. D. Hutcheon, N. P. Zaitseva, and J. J. De Yoreo, Proc. SPIE **2966**, 11 (1996).
22. G. Li, G. Zheng, Y. Qi, P. Yin, E. Tang, F. Li, J. Xu, T. Lei, X. Lin, M. Zhang, J. Lu, J. Ma, Y. He, and Y. Yao, High Power Laser Sci. **2**, e2 (2014).
23. J. M. Auerbach, P. J. Wegner, S. A. Couture, D. Eimerl, R. L. Hibbard, D. Milam, and L. A. Hackel, Appl. Opt. **40**, 1404 (2001).
24. D. Chen, B. Wang, H. Wang, L. Zheng, H. Zhang, H. Qi, and J. Shao, Cryst. Growth Des. **19**, 2746 (2019).
25. X. Xie, H. Qi, B. Wang, H. Wang, D. Chen, and J. Shao, J. Cryst. Growth **487**, 45 (2018).
26. G. Hu, Y. Wang, J. Chang, X. Xie, Y. Zhao, H. Qi, and J. Shao, High Power Laser Sci. **3**, e13 (2015).
27. H. F. Robey and D. Maynes, J. Cryst. Growth **222**, 263 (2001).
28. H. F. Robey, J. Cryst. Growth **259**, 388 (2003).
29. S. K. Sharma, S. Verma, Y. Singh, and K. S. Bartwal, CrystEngComm **15**, 9955 (2013).
30. X. Peng, Y. Zhao, Y. Wang, G. Hu, L. Yang, and J. Shao, Chin. Opt. Lett. **16**, 051601 (2018).
31. J. Wu, Y. Zhao, L. Wang, X. Peng, L. Yang, C. Shan, and J. Shao, Chin. J. Lasers **46**, 0501003 (2019).
32. S. P. Ramteke, M. Anis, M. I. Baig, H. Algarni, and G. G. Muley, Optik **197**, 163219 (2019).
33. M. Anis, M. I. Baig, M. S. Pandian, P. Ramasamy, S. AlFaify, V. Ganesh, G. G. Muley, and H. A. Ghramh, Cryst. Res. Technol. **53**, 1700165 (2018).
34. S. M. Azhar, M. Anis, G. Rabbani, M. D. Shirsat, M. I. Baig, S. S. Hussaini, S. AlFaify, and M. A. Khan, Optik **185**, 1247 (2019).
35. M. Anis, M. I. Baig, G. G. Muley, G. Rabbani, M. D. Shirsat, M. Shkir, and H. A. Ghramh, Mater. Lett. **233**, 238 (2018).
36. S. AlFaify, M. Shkir, V. Ganesh, M. Anis, and I. S. Yahia, Appl. Phys. B **124**, 196 (2018).
37. J. Y. Natoli, L. Gallais, H. Akhouayri, and C. Amra, Appl. Opt. **41**, 3156 (2002).
38. H. Krol, L. Gallais, C. Grezes-Besset, J. Y. Natoli, and M. Commandre, Opt. Commun. **256**, 184 (2005).
39. S. P. Ramteke, S. Kalainathan, M. Anis, G. G. Muley, M. I. Baig, and H. Algarni, Optik **201**, 163509 (2020).
40. S. P. Ramteke, M. I. Baig, M. Shkir, S. Kalainathan, M. D. Shirsat, G. G. Muley, and M. Anis, Opt. Laser Technol. **104**, 83 (2018).
41. S. M. Azhar, S. S. Hussaini, M. D. Shirsat, G. Rabbani, M. Shkir, S. Alfaify, H. A. Ghramh, M. I. Baig, and M. Anis, Mater. Res. Innov. **23**, 123 (2019).
42. G. Hu, Y. Zhao, D. Li, and Q. Xiao, Chin. Phys. Lett. **29**, 037801 (2012).
43. C. W. Carr, M. D. Feit, M. A. Johnson, and A. M. Rubenchik, Appl. Phys. Lett. **89**, 131901 (2006).
44. A. K. Burnham, M. Runkel, M. D. Feit, A. M. Rubenchik, R. L. Floyd, T. A. Land, W. J. Siekhaus, and R. A. Hawley-Fedder, Appl. Opt. **42**, 5483 (2003).
45. H. Jiang, J. McNary, H. W. K. Tom, M. Yan, H. B. Radousky, and S. G. Demos, Appl. Phys. Lett. **81**, 3149 (2002).
46. H. Yoshida, T. Jitsuno, H. Fujita, M. Nakatsuka, M. Yoshimura, T. Sasaki, and K. Yoshida, Appl. Phys. B **70**, 195 (2000).
47. P. DeMange, C. W. Carr, H. B. Radousky, and S. G. Demos, Proc. SPIE **5337**, 47 (2004).